

Modeling Continuous Stochastic Processes with Dynamic Normalizing Flows

Ruizhi Deng^{1,2,*} Bo Chang² Marcus A. Brubaker^{2,3} Greg Mori^{1,2} Andreas Lehrmann²

Abstract

Normalizing flows transform a simple base distribution into a complex target distribution and have proved to be powerful models for data generation and density estimation. In this work, we propose a novel type of normalizing flow driven by a differential deformation of the continuous-time Wiener process. As a result, we obtain a rich time series model whose observable process inherits many of the appealing properties of its base process, such as efficient computation of likelihoods and marginals. Furthermore, our continuous treatment provides a natural framework for irregular time series with an independent arrival process, including straightforward interpolation. We illustrate the desirable properties of the proposed model on popular stochastic processes and demonstrate its superior flexibility to variational RNN and latent ODE baselines in a series of experiments on synthetic and real-world data.

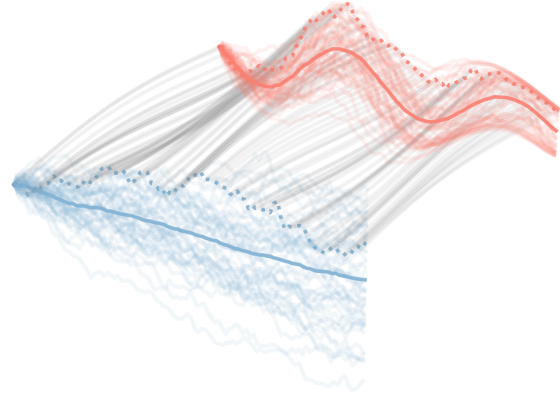


Figure 1. Overview. Wiener processes are continuous-time stochastic processes with appealing properties but limited flexibility. We propose to learn complex observed processes (red) through continuous deformations (grey) of latent Wiener processes (blue) with dynamic normalizing flows, thereby preserving the advantages of the base process.

1. Introduction

Expressive models for sequential data form the statistical basis for downstream tasks in a wide range of domains, including computer vision, robotics, and finance. Recent advances in deep generative architectures, and especially the concept of reversibility, have led to tremendous progress in this area and created a new perspective on many of the long-standing capacitive limitations that are typical in traditional approaches based on structured decompositions (e.g., state-space models). The increased flexibility of these approaches does not come without a price, though, and some of the appealing properties of traditional time series models, such as their probabilistic rigor and well-defined statistics, must be sacrificed.

We argue that the power of a time series model depends on its properties in the following areas: (1 – Resolution) The majority of time series models are discrete with respect

to time. As a result, they make the implicit assumption of a uniformly spaced temporal grid, which precludes their application from asynchronous tasks with a separate arrival process; (2 – Structural assumptions) The expressiveness of a temporal model is determined by the dependencies and shapes of its variables. In particular, the topological structure should be rich enough to capture the dynamics of the underlying process but sparse enough to allow for robust learning and efficient inference. The distributions must find a similar balance in terms of their parametric assumptions; (3 – Generation) A good time series model must be able to generate unbiased samples from the true underlying process in an efficient way; (4 – Inference) Given a trained model, it should support standard inference tasks, such as interpolation, forecasting and likelihood calculation.

Over the years, a plethora of attempts have been made to strike this bias-variance trade-off and deal with the resulting implications for generation and inference. Traditional time series models often make strong parametric assumptions about the shape and connectivity of the underlying process, which typically results in straightforward generation and inference but limits their applicability in tasks with non-stationary dynamics or complex uncertainty. Attempts to increase the capacity of these models typically

* Work done during an internship at Borealis AI. ¹Simon Fraser University ²Borealis AI ³York University. Correspondence to: Ruizhi Deng <wsdmdeng@gmail.com>.

result in expensive inference based on Monte Carlo techniques. More recently, deep generative modeling has enabled vastly increased flexibility while keeping generation and inference tractable, owing to novel techniques like amortized variational inference (Kingma & Welling, 2014; Chung et al., 2015), reversible generative models (Rezende & Mohamed, 2015; Kingma & Dhariwal, 2018), and differential networks (Chen et al., 2018; Li et al., 2020).

In this work, we approach the modeling of continuous and irregular time series with a *reversible generative model for stochastic processes*. Our approach builds upon ideas from normalizing flows; however, instead of a static base distribution, we transform a dynamic base process into an observable one. In particular, we introduce *continuous-time flow processes (CTFPs)*, a novel type of generative model that decodes a latent Wiener process into a complex observable process using a dynamic instance of normalizing flows. Due to the tractable Jacobians of the generating flow, many appealing properties of the Wiener process directly propagate to the observable process. In addition to the static properties of normalizing flows (e.g., efficient sampling, exact likelihood), this also includes a series of inference tasks that are typically unattainable in time series models with complex dynamics, such as interpolation and forecasting at arbitrary real-valued points. Furthermore, to overcome the simple covariance structure of a Wiener process, we augment the reversible mapping with latent variables and show how to optimize this latent CTFP variant using variational optimization. Both CTFP and latent CTFP use a novel generative instance of the *augmented neural ordinary differential equation* (ANODE; Dupont et al. 2019).

Contributions. In summary, we make the following contributions: (1) we extend the concept of normalizing flows from base distributions to base processes; (2) we describe efficient sampling and inference schemes based on a propagation of the tractable dynamics of a latent Wiener process to an expressive observable process; (3) we propose a modified ANODE model that can be used as a generative model; (4) we validate our approach on a series of common stochastic processes and real-world datasets and show superior performance w.r.t. state-of-the-art methods based on variational recurrent neural networks (VRNN; Chung et al. 2015) and latent ordinary differential equations (latent ODE; Rubanova et al. 2019).

2. Related Work

Our approach builds upon prior research on stochastic processes, normalizing flows, continuous neural networks, and variational inference. The following sections discuss the relevant literature in these areas and put them in context with the proposed model.

2.1. Early Work

Among the most popular traditional time series models are latent variable models following the state-space equations (Durbin & Koopman, 2012), including the well-known variants with discrete and linear state-space (Baum & Petrie, 1966; Kalman, 1960). In the non-linear case, exact inference is typically intractable and we need to resort to approximate techniques (Julier & Uhlmann, 1997; Ito & Xiong, 2000; Capp et al., 2005; 2007). Tree-based variants of non-linear Markov models have been proposed in Lehmann et al. (2014). An augmentation with switching states increases the expressiveness of state-space models but introduces additional challenges for learning (Fox et al., 2008) and inference (Barber, 2012). An early solution to switching systems based on variational inference was proposed in Pavlovic et al. (2000). Marginalization over an expansion of the state-space equations in terms of non-linear basis functions extends classical Gaussian processes (Rasmussen, 2006) to Gaussian process dynamical models (J.M. Wang et al., 2008), which can be learned via hybrid Monte Carlo (Duane et al., 1987). With very few exceptions (Srkk, 2007), time is assumed to be discrete in these models.

2.2. Stochastic Processes

A stochastic process can be defined as a collection of random variables that are indexed by time. The standard approach to defining a stochastic process is via its finite-dimensional marginal distributions. The Kolmogorov extension theorem states that if the exchangeability and consistency conditions are satisfied, then a collection of finite-dimensional distributions defines a stochastic process. See the supplementary materials for more details about the Kolmogorov extension theorem.

An example of a continuous-time stochastic process is the *Wiener process*. It is also known as the *Brownian motion* due to its historical connection with the physical process of the same name. We refer the readers to any textbook on stochastic processes, e.g., Grimmett et al. (2001), for the construction and properties of the Wiener process.

The d -dimensional Wiener process \mathbf{W}_τ can be characterized by the following properties: (1) $\mathbf{W}_0 = 0$; (2) $\mathbf{W}_t - \mathbf{W}_s \sim \mathcal{N}(0, (t - s)\mathbf{I}_d)$ for $s \leq t$, and $\mathbf{W}_t - \mathbf{W}_s$ is independent of past values of $\mathbf{W}_{s'}$ for all $s' \leq s$. This is known as the *independent increments property*. As a result, the joint density of $(\mathbf{W}_{\tau_1}, \dots, \mathbf{W}_{\tau_n})$ can be written as the product of the conditional densities: $p_{(\mathbf{W}_{\tau_1}, \dots, \mathbf{W}_{\tau_n})}(\mathbf{w}_{\tau_1}, \dots, \mathbf{w}_{\tau_n}) = \prod_{i=1}^n p_{\mathbf{W}_{\tau_i} | \mathbf{W}_{\tau_{i-1}}}(\mathbf{w}_{\tau_i} | \mathbf{w}_{\tau_{i-1}})$ for $0 \leq \tau_1 < \dots < \tau_n \leq T$.

The conditional distribution of $p_{\mathbf{W}_t | \mathbf{W}_s}$, for $s < t$, is multivariate Gaussian; its conditional density is

$$p_{\mathbf{W}_t | \mathbf{W}_s}(\mathbf{w}_t | \mathbf{w}_s) = \mathcal{N}(\mathbf{w}_t; \mathbf{w}_s, (t - s)\mathbf{I}_d), \quad (1)$$

where \mathbf{I}_d is a d -dimensional identity matrix. This equation also provides a way to sample from $(\mathbf{W}_{\tau_1}, \dots, \mathbf{W}_{\tau_n})$. Furthermore, given $\mathbf{W}_{t_1} = \mathbf{w}_{t_1}$ and $\mathbf{W}_{t_2} = \mathbf{w}_{t_2}$, the conditional distribution of \mathbf{W}_t for $t_1 \leq t \leq t_2$ is also Gaussian:

$$p_{\mathbf{W}_t | \mathbf{W}_{t_1}, \mathbf{W}_{t_2}}(\mathbf{w}_t | \mathbf{w}_{t_1}, \mathbf{w}_{t_2}) = \mathcal{N}\left(\mathbf{w}_t; \mathbf{w}_{t_1} + \frac{t - t_1}{t_2 - t_1}(\mathbf{w}_{t_2} - \mathbf{w}_{t_1}), \frac{(t_2 - t)(t - t_1)}{t_2 - t_1} \mathbf{I}_d\right). \quad (2)$$

This is known as the (general) Brownian bridge.

Another property of the Wiener process is that the trajectories sampled from the Wiener process are continuous in time almost surely. Many time series data can be regarded as finite-dimensional observations of a sampled trajectory from a continuous-time stochastic process, e.g., weather, power consumption, etc.

2.3. Normalizing Flows

Normalizing flows are reversible generative models that allow both density estimation and sampling. They map a simple distribution to a complex one using a bijective function. Specifically, if our interest is to estimate the density function $p_{\mathbf{X}}$ of a random vector $\mathbf{X} \in \mathbb{R}^d$, then normalizing flows assume $\mathbf{X} = f(\mathbf{Z})$, where $f : \mathbb{R}^d \rightarrow \mathbb{R}^d$ is a bijective function, and $\mathbf{Z} \in \mathbb{R}^d$ is a random vector with a simple density function $p_{\mathbf{Z}}$. We further denote the inverse of f by g . On the one hand, the probability density function can be evaluated using the change of variables formula:

$$\log p_{\mathbf{X}}(\mathbf{x}) = \log p_{\mathbf{Z}}(g(\mathbf{x})) + \log \left| \det \left(\frac{\partial g}{\partial \mathbf{x}} \right) \right|, \quad (3)$$

where $\partial g / \partial \mathbf{x}$ denotes the Jacobian matrix of g . On the other hand, sampling from $p_{\mathbf{X}}$ can be done by first drawing a sample from the simple distribution $\mathbf{z} \sim p_{\mathbf{Z}}$, and then apply the bijection $\mathbf{x} = f(\mathbf{z})$.

It is natural to construct f as a neural network, however, it requires the bijection f to be invertible, and the determinant of the Jacobian matrix should be efficient to compute. Several methods have been proposed along this research direction (Rezende & Mohamed, 2015; Dinh et al., 2014; Kingma et al., 2016; Dinh et al., 2017; Papamakarios et al., 2017; Kingma & Dhariwal, 2018; Behrmann et al., 2019; Chen et al., 2019). We refer the readers to Kobyzev et al. (2019); Papamakarios et al. (2019) for extensive overviews of normalizing flow models.

2.4. Continuous Normalizing Flows

Instead of modeling the bijective mapping as a neural network, an alternative is to use the *continuous normalizing flow*, or *neural ordinary differential equation* (neural ODE;

Chen et al. 2018; Grathwohl et al. 2019). Given $\mathbf{z} = \mathbf{h}(t_0)$ sampled from the base distribution $p_{\mathbf{Z}}$, it is mapped to $\mathbf{h}(t_1)$ based on the mapping defined by the ordinary differential equation (ODE): $d\mathbf{h}(t)/dt = f(\mathbf{h}(t), t)$. The change in log-density is computed by the *instantaneous change of variables formula* (Chen et al., 2018):

$$\log p_{\mathbf{X}}(\mathbf{h}(t_1)) = \log p_{\mathbf{Z}}(\mathbf{h}(t_0)) - \int_{t_0}^{t_1} \text{tr} \left(\frac{\partial f}{\partial \mathbf{h}(t)} \right) dt. \quad (4)$$

During training, the ODE is run in the backward direction from t_1 to t_0 to maximize the likelihood of observations.

One potential disadvantage of the neural ODE model is that it preserves the topology of the input space. As a result, there are classes of functions that cannot be represented by neural ODEs. Dupont et al. (2019) propose the augmented neural ODE (ANODE) model to address this limitation. ANODEs augment the space on which the ODE is solved, leading to more expressive, stable, and computationally efficient models.

Note that the original formulation of ANODE only supports the computation of likelihood $p_{\mathbf{X}}(\mathbf{x})$, but not sampling from the target distribution $\mathbf{x} \sim p_{\mathbf{X}}$. In this work, we propose a modified version of ANODE that can be used as (conditional) generative model.

2.5. Variational Sequence Models

Latent variable models assume the data are generated from some low-dimensional or sparse latent variables $\mathbf{Z} \sim p_{\mathbf{Z}}$, and define a conditional distribution $p_{\mathbf{X}|\mathbf{Z}}$, where \mathbf{X} denotes the observed variables. The latent variables can often help generative models find the underlying structures and capture more probability distributions of $p_{\mathbf{X}}$. However, the posterior distribution $p_{\mathbf{Z}|\mathbf{X}}$ is often intractable. Variational autoencoders (VAE; Kingma & Welling 2014) introduce a variational distribution $q_{\mathbf{Z}|\mathbf{X}}$ to approximate the intractable posterior distribution and maximize the evidence lower bound (ELBO) or the importance weighted autoencoder (IWAE; Burda et al. 2019) lower bound of the marginal log-likelihood of data.

VAEs have demonstrated impressive performance on non-sequential data like images. Many following works (Bowman et al., 2015; Chung et al., 2015; Fraccaro et al., 2016; Luo et al., 2018) extend the domain of VAE models to sequential data. More recently, latent ODE (Rubanova et al., 2019) uses the ODE-RNN as encoders and neural ODE as decoders. The neural stochastic differential equation (SDE) models the latent process as an SDE (Li et al., 2020). Furthermore, motivated by neural process models (Garnelo et al., 2018a;b; Kim et al., 2019), Singh et al. (2019) propose the sequential neural process model.

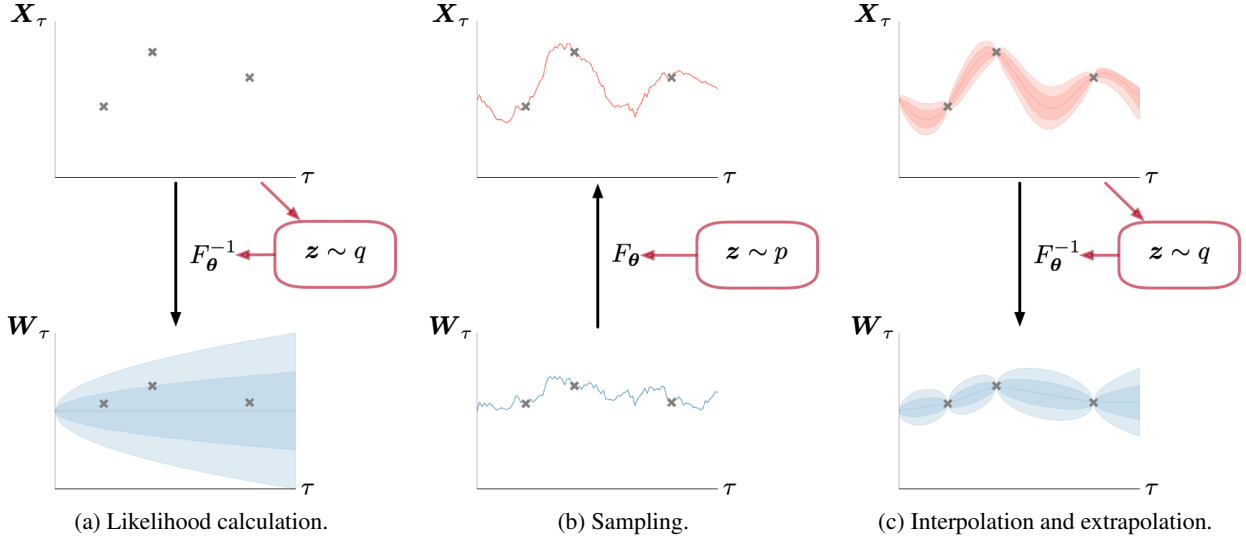


Figure 2. (Latent) Continuous-Time Flow Processes (CTFPs). (a) Likelihood calculation. Given an irregular time series $\{x_{\tau_i}\}$, the inverse flow F_{θ}^{-1} maps the observed process to a set of Wiener points $\{w_{\tau_i}\}$ for which we can compute the likelihood according to Equation 8. (b) Sampling. Given a set of timestamps $\{\tau_i\}$, we sample a Wiener process according to Equation 1 and use the forward flow F_{θ} to obtain a sample of the observed process. (c) Interpolation and extrapolation. In order to compute the density at an unobserved point x_{τ} , we compute the left-sided (extrapolation; Equation 1) or two-sided (interpolation; Equation 2) conditional density of its Wiener point w_{τ} and adjust for the flow (Equation 12). **Notes:** The effect of the latent variables Z in our latent CTFP model is indicated by red boxes. The shaded areas represent 70% and 95% confidence intervals.

3. Model

In Section 3.1, we introduce a modified variant of ANODE that can be used as a conditional generative model. The modified ANODE is then used as part of the *continuous-time flow process (CTFP)* defined in Section 3.2. Next, Section 3.3 describes how to perform interpolation and extrapolation on time series data using the proposed model. Finally, we present the latent CTFP model in Section 3.4.

3.1. Modified ANODE

Following a similar design as the ANODE, we augment the continuous normalizing flow $h(t)$ with conditional variables a_0 and define an augmented initial value problem:

$$\frac{d}{dt} \begin{pmatrix} h(t) \\ a(t) \end{pmatrix} = \begin{pmatrix} f(h(t), a(t), t) \\ g(a(t), t) \end{pmatrix}, \quad \begin{pmatrix} h(t_0) \\ a(t_0) \end{pmatrix} = \begin{pmatrix} h_0 \\ a_0 \end{pmatrix}, \quad (5)$$

for $t \in [t_0, t_1]$. The initial value problem can be solved from t_0 to t_1 , i.e., in the forward direction. For the backward direction, given $h(t_1)$ and the conditional variables $a_0 = a(t_0)$, we first solve the ODE for $a(t)$ for $t \in [t_0, t_1]$, and then solve for $h(t_0)$. In other words, given the conditional variables, the modified ANODE is able to run in both directions. As a result, it can be used as a conditional generative model.

With the definition of this modified ANODE model, we are

ready to introduce our CTFP model.

3.2. Continuous-Time Flow Process

The observed data is an irregularly spaced time series, denoted by $\{(x_{\tau_i}, \tau_i)\}_{i=1}^n$, where $x_{\tau_i} \in \mathbb{R}^d$ represents the observed variables and $\tau_i \in [0, T]$ is the corresponding timestamp which satisfies $\tau_i < \tau_j$ for all $i < j$. We assume the time series to be an (incomplete) realization of a continuous stochastic process $\{X_{\tau}\}_{\tau \in [0, T]}$. The goal is to model $\{X_{\tau}\}_{\tau \in [0, T]}$ such that the log-likelihood on the observations

$$\mathcal{L} = \log p_{X_{\tau_1}, \dots, X_{\tau_n}}(x_{\tau_1}, \dots, x_{\tau_n}) \quad (6)$$

is maximized. The distribution of X_{τ} is modeled by a normalizing flow model F_{θ} such that

$$X_{\tau} = F_{\theta}(W_{\tau}; \tau), \quad \forall \tau \in [0, T], \quad (7)$$

where $F_{\theta}(\cdot; \tau) : \mathbb{R}^d \rightarrow \mathbb{R}^d$ is an invertible mapping parametrized by the learnable parameters θ and time τ , and W_{τ} is a d -dimensional Wiener process. As a result, the joint distribution of $(X_{\tau_1}, \dots, X_{\tau_n})$ is the same as that of $(F_{\theta}(W_{\tau_1}; \tau_1), \dots, F_{\theta}(W_{\tau_n}; \tau_n))$.

This probability distribution of $(X_{\tau_1}, \dots, X_{\tau_n})$ is well defined as it satisfies the conditions of the Kolmogorov extension theorem in the supplementary materials. It is worth noting that given a continuous realization of W_{τ} , as long

as $F_\theta(\cdot; \tau)$ is implemented as a continuous mapping, the resulting trajectory \mathbf{x}_τ is also continuous. In other words, this formulation allows us to sample continuous trajectories from $\{\mathbf{X}_\tau\}_{\tau \in [0, T]}$.

The log-likelihood in Equation 6 can be rewritten using the change of variables formula. Let $\mathbf{w}_{\tau_i} = F_\theta^{-1}(\mathbf{x}_{\tau_i}; \tau_i)$, then

$$\begin{aligned} \mathcal{L} &= \log p_{\mathbf{X}_{\tau_1}, \dots, \mathbf{X}_{\tau_n}}(\mathbf{x}_{\tau_1}, \dots, \mathbf{x}_{\tau_n}) \\ &= \log p_{\mathbf{W}_{\tau_1}, \dots, \mathbf{W}_{\tau_n}}(\mathbf{w}_{\tau_1}, \dots, \mathbf{w}_{\tau_n}) \\ &\quad - \log \left| \det \frac{\partial(\mathbf{x}_{\tau_1}, \dots, \mathbf{x}_{\tau_n})}{\partial(\mathbf{w}_{\tau_1}, \dots, \mathbf{w}_{\tau_n})} \right| \\ &= \sum_{i=1}^n \left[\log p_{\mathbf{W}_{\tau_i} | \mathbf{W}_{\tau_{i-1}}}(\mathbf{w}_{\tau_i} | \mathbf{w}_{\tau_{i-1}}) - \log \left| \det \frac{\partial \mathbf{x}_{\tau_i}}{\partial \mathbf{w}_{\tau_i}} \right| \right], \end{aligned} \quad (8)$$

where $\tau_0 = 0$, $\mathbf{W}_0 = 0$, and $p_{\mathbf{W}_{\tau_i} | \mathbf{W}_{\tau_{i-1}}}$ is defined in Equation 1. When $n = 1$, the joint distribution degenerates to the marginal distribution of \mathbf{X}_{τ_1} . Figure 2a shows an example of the likelihood calculation.

Using the modified ANODE model defined in Section 3.1 as the invertible mapping F_θ , we introduce the continuous-time flow process (CTFP) model. For any fixed $\tau \in [0, T]$ and $\mathbf{w}_\tau \in \mathbb{R}^d$, consider the following initial value problem:

$$\begin{aligned} \frac{d}{dt} \begin{pmatrix} \mathbf{h}_\tau(t) \\ \mathbf{a}_\tau(t) \end{pmatrix} &= \begin{pmatrix} f_\theta(\mathbf{h}_\tau(t), \mathbf{a}_\tau(t), t) \\ g_\theta(\mathbf{a}_\tau(t), t) \end{pmatrix}, \\ \begin{pmatrix} \mathbf{h}_\tau(t_0) \\ \mathbf{a}_\tau(t_0) \end{pmatrix} &= \begin{pmatrix} \mathbf{w}_\tau \\ \tau \end{pmatrix}, \end{aligned} \quad (9)$$

where $\mathbf{h}_\tau(t) \in \mathbb{R}^d$, $t \in [t_0, t_1]$, $f_\theta : \mathbb{R}^d \times \mathbb{R} \times [t_0, t_1] \rightarrow \mathbb{R}^d$, and $g_\theta : \mathbb{R} \times [t_0, t_1] \rightarrow \mathbb{R}$. Then F_θ in Equation 7 is defined as the solution of $\mathbf{h}_\tau(t)$ at $t = t_1$:

$$\begin{aligned} F_\theta(\mathbf{w}_\tau; \tau) &:= \mathbf{h}_\tau(t_1) \\ &= \mathbf{h}_\tau(t_0) + \int_{t_0}^{t_1} f_\theta(\mathbf{h}_\tau(t), \mathbf{a}_\tau(t), t) dt. \end{aligned} \quad (10)$$

Note that the index t represents the independent variable in the initial value problem and should not be confused with τ , the timestamp of the observation.

Using the instantaneous change of variables formula in Equation 4, the log-likelihood \mathcal{L} can be calculated as follows:

$$\begin{aligned} \mathcal{L} &= \sum_{i=1}^n \left[\log p_{\mathbf{W}_{\tau_i} | \mathbf{W}_{\tau_{i-1}}}(\mathbf{h}_{\tau_i}(t_0) | \mathbf{h}_{\tau_{i-1}}(t_0)) \right. \\ &\quad \left. - \int_{t_0}^{t_1} \text{tr} \left(\frac{\partial f_\theta(\mathbf{h}_{\tau_i}(t), \mathbf{a}_{\tau_i}(t), t)}{\partial \mathbf{h}_{\tau_i}(t)} \right) dt \right], \end{aligned} \quad (11)$$

where $\mathbf{h}_{\tau_i}(t_0)$ is obtained by solving the ODE in Equation 9 backwards from $t = t_1$ to $t = t_0$, and the trace of

the Jacobian can be estimated by Hutchinsons trace estimator (Hutchinson, 1990; Grathwohl et al., 2019).

Sampling from a CTFP is straightforward. Given the timestamps τ_i , we first sample a realization of the Wiener process $\{\mathbf{w}_{\tau_i}\}_{i=1}^n$ using Equation 1, then map them to $\mathbf{x}_{\tau_i} = F_\theta(\mathbf{w}_{\tau_i})$. Figure 2b illustrates this procedure.

3.3. Interpolation and Extrapolation with CTFP

Apart from likelihood calculation and sampling, the CTFP model can also perform interpolation and extrapolation, which are important tasks in time series modeling.

Interpolation means that we can model the conditional distribution $p_{\mathbf{X}_\tau | \mathbf{X}_{\tau_i}, \mathbf{X}_{\tau_{i+1}}}(\mathbf{x}_\tau | \mathbf{x}_{\tau_i}, \mathbf{x}_{\tau_{i+1}})$ for all $\tau \in [\tau_i, \tau_{i+1}]$ and $i = 1, \dots, n-1$. This can be done by mapping the values \mathbf{x}_τ , \mathbf{x}_{τ_i} and $\mathbf{x}_{\tau_{i+1}}$ to \mathbf{w}_τ , \mathbf{w}_{τ_i} and $\mathbf{w}_{\tau_{i+1}}$, respectively. After that, Equation 2 can be applied to obtain the conditional density of $p_{\mathbf{W}_\tau | \mathbf{W}_{\tau_1}, \mathbf{W}_{\tau_2}}(\mathbf{w}_\tau | \mathbf{w}_{\tau_1}, \mathbf{w}_{\tau_2})$. Finally, we have

$$\begin{aligned} &\log p_{\mathbf{X}_\tau | \mathbf{X}_{\tau_i}, \mathbf{X}_{\tau_{i+1}}}(\mathbf{x}_\tau | \mathbf{x}_{\tau_i}, \mathbf{x}_{\tau_{i+1}}) \\ &= \log p_{\mathbf{W}_\tau | \mathbf{W}_{\tau_i}, \mathbf{W}_{\tau_{i+1}}}(\mathbf{w}_\tau | \mathbf{w}_{\tau_i}, \mathbf{w}_{\tau_{i+1}}) - \log \left| \frac{\partial \mathbf{x}_\tau}{\partial \mathbf{w}_\tau} \right|. \end{aligned} \quad (12)$$

Extrapolation can be done in a similar fashion using Equation 1. This allows the model to predict continuous trajectories into the future, given past observations. Figure 2c shows a visualization of interpolation and extrapolation using CTFP.

3.4. Latent Continuous-Time Flow Process

The CTFP model inherits the independent increments property from the Wiener process, which is a strong assumption and limits its ability to model stochastic processes with complex temporal dependence. In order to enhance the expressive power of the CTFP model, we augment it with a latent variable $\mathbf{Z} \in \mathbb{R}^m$, whose prior distribution is an isotropic Gaussian $p_{\mathbf{Z}}(\mathbf{z}) = \mathcal{N}(\mathbf{z}; 0, \mathbf{I}_m)$. As a result, the data distribution can be approximated by a diverse collection of CTFP models conditioned on sampled latent variables \mathbf{z} .

The generative model in Equation 7 is augmented to

$$\mathbf{X}_\tau = F_\theta(\mathbf{W}_\tau; \mathbf{Z}, \tau), \quad \forall \tau \in [0, T], \quad (13)$$

which induces the conditional distribution $\mathbf{X}_{\tau_1}, \dots, \mathbf{X}_{\tau_n} | \mathbf{Z}$. Similar to the initial value problem in Equation 9, we define $F_\theta(\mathbf{w}_\tau; \mathbf{z}, \tau) = \mathbf{h}_\tau(t_1)$, where

$$\begin{aligned} \frac{d}{dt} \begin{pmatrix} \mathbf{h}_\tau(t) \\ \mathbf{a}_\tau(t) \end{pmatrix} &= \begin{pmatrix} f_\theta(\mathbf{h}_\tau(t), \mathbf{a}_\tau(t), t) \\ g_\theta(\mathbf{a}_\tau(t), t) \end{pmatrix}, \\ \begin{pmatrix} \mathbf{h}_\tau(t_0) \\ \mathbf{a}_\tau(t_0) \end{pmatrix} &= \begin{pmatrix} \mathbf{w}_\tau \\ (\mathbf{z}, \tau)^\top \end{pmatrix}. \end{aligned} \quad (14)$$

Depending on the sample of the latent variable z , the CTFP model has different gradient fields and thus different output distributions.

For simplicity of notation, the subscripts of density functions are omitted from now on. For the augmented generative model, the log-likelihood becomes

$$\mathcal{L} = \log \int_{\mathbb{R}^m} p(\mathbf{x}_{\tau_1}, \dots, \mathbf{x}_{\tau_n} | z) p(z) dz, \quad (15)$$

which is intractable to evaluate. Following the variational autoencoder approach (Kingma & Welling, 2014), we introduce an approximate posterior distribution of $Z | \mathbf{X}_{\tau_1}, \dots, \mathbf{X}_{\tau_n}$, denoted by $q(z | \mathbf{x}_{\tau_1}, \dots, \mathbf{x}_{\tau_n})$. The implementation of the approximate posterior distribution is the ODE-RNN encoder proposed in Rubanova et al. (2019).

With the approximate posterior distribution, we can derive an importance-weighted autoencoder (IWAE) lower bound of the log-likelihood (Burda et al., 2019):

$$\begin{aligned} \mathcal{L} &= \log \mathbb{E}_{z \sim q} \left[\frac{p(\mathbf{x}_{\tau_1}, \dots, \mathbf{x}_{\tau_n} | z) p(z)}{q(z | \mathbf{x}_{\tau_1}, \dots, \mathbf{x}_{\tau_n})} \right] \\ &\geq \mathbb{E}_{z_k \sim q} \left[\log \left(\frac{1}{K} \sum_{k=1}^K \frac{p(\mathbf{x}_{\tau_1}, \dots, \mathbf{x}_{\tau_n} | z_k) p(z_k)}{q(z_k | \mathbf{x}_{\tau_1}, \dots, \mathbf{x}_{\tau_n})} \right) \right] \\ &=: \mathcal{L}_{\text{IWAE}}, \end{aligned} \quad (16)$$

where K is the number of samples from the approximate posterior distribution.

4. Experiments

In this section, we apply our models on synthetic data generated from common continuous-time stochastic processes and complex real-world datasets. The proposed CTFP and latent CTFP models are compared against two baseline models: latent ODE (Rubanova et al., 2019) and variational RNNs (VRNNs; Chung et al. 2015). The latent ODE model belongs to the family of neural process models and is designed specifically to model time series data with irregular observation times. The VRNN model is a popular model for sequential data. However, the probability distribution modeled by VRNNs on an arbitrary time grid is not guaranteed to be well-defined as it does not necessarily satisfy the conditions in the Kolmogorov extension theorem.

For VRNNs, we append the time gaps between two observations as an additional input to the neural network. Both latent CTFP and latent ODE models use ODE-RNN (Rubanova et al., 2019) as the inference network; GRU (Cho et al., 2014) is used as the RNN cell in latent CTFP, latent ODE, and VRNN models. All three latent-variable models have the same latent dimension and GRU hidden state dimension. Please refer to the supplementary materials for more details of our experimental setups and model implementations.

4.1. Synthetic Datasets

We simulate three irregularly-sampled time series datasets; all of them are univariate, i.e., $d = 1$.

Geometric Brownian motion (GBM) is a continuous-time stochastic process widely used in mathematical finance. It satisfies the following stochastic differential equation:

$$dX_\tau = \mu X_\tau d\tau + \sigma X_\tau dW_\tau, \quad (17)$$

where μ and σ are the drift term and variance term, respectively. We sample trajectories from a GBM with a drift of $\mu = 0.2$ and a variance of $\sigma = 0.5$. The timestamps of the observations are in the range between 0 and $T = 30$ and are sampled from a homogeneous Poisson point process with an intensity of $\lambda_{\text{train}} = 0.5$. To further evaluate the model’s capacity to capture the dynamics of GBM, we test the model with observation time-steps sampled from Poisson point processes with intensities of $\lambda_{\text{test}} = 0.5$ and $\lambda_{\text{test}} = 20$.

Ornstein–Uhlenbeck process (OU Process) is another type of widely used continuous-time stochastic process. The OU process satisfies the following stochastic differential equation:

$$dX_\tau = \theta(\mu - X_\tau) d\tau + \sigma dW_\tau. \quad (18)$$

We compare our CTFP and latent CTFP models against the baseline models on fitting an OU process with the following parameters: $\theta = 2$, $\mu = 1$, and $\sigma = 10$. We train the models with sequences that have denser observations than GBM experiments. Observation timestamps in the training set are sampled from a Poisson process with intensity of $\lambda_{\text{train}} = 2$. We test the model with observation time-steps sampled from a Poisson point processes with intensities of $\lambda_{\text{test}} = 0.5$ and $\lambda_{\text{test}} = 20$.

Mixture of GBMs To demonstrate the latent CTFP’s capability to model sequences sampled from different continuous-time stochastic processes, we train the models on a dataset generated by mixing the sequences sampled from two different GBM processes. Half of the sequences in the dataset are sampled from a GBM with $\sigma = 0.5$ and a sampling intensity of $\lambda_{\text{train}} = 1$. The other half are sampled from a GBM with $\sigma = 2$ and a sampling intensity of $\lambda_{\text{train}} = 20$. The test set has the same sampling intensities as the training set.

The results are presented in Table 1. We report the exact negative log-likelihood (NLL) per observation for CTFP. For latent ODE, latent CTFP, and VRNN, we report the (upper bound of) NLL estimated by IWAE bound (Burda et al., 2019) in Equation 16, using $K = 25$ samples of latent variables. Empirically, we find $K = 25$ samples are sufficient for the estimation to converge. In addition to the baseline models, we also show the NLL of the test set

Model	Negative Log-Likelihood				
	GBM		OU		M-GBM
	$\lambda_{\text{test}} = 0.5$	$\lambda_{\text{test}} = 20$	$\lambda_{\text{test}} = 2$	$\lambda_{\text{test}} = 20$	$\lambda_{\text{test}} = (1, 20)$
Latent ODE (Rubanova et al., 2019)	4.992	4.934	3.066	3.027	2.380
VRNN (Chung et al., 2015)	4.096	3.166	2.729	1.939	2.517
CTFP (ours)	3.786	1.929	2.903	1.942	-0.742
Latent CTFP (ours)	3.784	1.943	2.902	1.936	-0.835
Ground Truth	3.783	1.928	2.722	1.888	-0.848

Table 1. **Quantitative Evaluation (Synthetic Data)**. We show test negative log-likelihood on three synthetic stochastic processes across different models. Below each process, we indicate the intensity of the Poisson point process from which the timestamps for the test sequences were sampled. “Ground Truth” refers to the closed-form negative log-likelihood of the true underlying data generation process. [GBM: geometric Brownian motion; OU: OrnsteinUhlenbeck process; M-GBM: mixture of GBMs.]

computed with the ground truth density function of each stochastic process as a reference.

The results on the test set sampled from the GBM indicate that the CTFP model can recover the true data generation process as the NLL estimated by CTFP is close to the ground truth. In contrast, latent ODE and VRNN models fail to recover the true data distribution. On the M-GBM dataset, CTFP and latent CTFP models show significantly better performance than other models. Moreover, latent CTFP can leverage the latent variables and outperform CTFP by 0.1 nats.

For the dataset sampled from the OU process, even though CTFP and latent CTFP models slightly underfit the data with $\lambda_{\text{test}} = 2$, they can adapt to a denser observation process with $\lambda_{\text{test}} = 20$ and make better density estimation. On the other hand, VRNN achieves better NLL values with $\lambda_{\text{test}} = 2$, but it does not recover the true OU process when λ_{test} increases to 20. This gap shows VRNN models have difficulty generalizing to different observation processes when modeling continuous-time stochastic processes. It also indicates that the finite-dimensional joint distribution of observations on an arbitrary set of timestamps is not well defined by VRNN models.

Figure 3 provides qualitative results of a CTFP model trained on the GBM synthetic dataset. The top row corresponds to the CTFP model, and the bottom row represents the geometric Brownian motion on which our model is trained. We show the estimated marginal density, inter-quartile range, and mean. All the estimates are accurate and consistent with the ground truth model.

4.2. Real-World Datasets

Our models are also evaluated on real-world datasets with various dynamics and complexities. The datasets consist of synchronous time series sequences. We first pad all the sequences in each dataset to the same length and rescale

the indices of the observation into $[0, 120]$. To make the sequences asynchronous or irregularly-sampled, we sample observation timestamps $\{\tau_i\}_{i=1}^n$ from a homogeneous Poisson point process. For each sampled timestamp, the value of the closest observation is taken as its corresponding value.

The following three datasets are considered: **Mujoco-Hopper** (Rubanova et al., 2019) consists of 10,000 sequences that are simulated by a “Hopper” model from the DeepMind Control Suite in a MuJoCo environment (Tassa et al., 2018). The dataset is 14-dimensional, and the length of each sequence is 200. The initial position and velocity of the hopper are randomly sampled. The trajectories are deterministic functions of their initial states. **PTB Diagnostic Database** (PTBDB; Bousseljot et al. 1995) consists of excerpts of ambulatory electrocardiography (ECG) recordings. Each sequence is one-dimensional, and the sampling frequency of the recordings is 125 Hz. **Beijing Air-Quality Dataset** (BAQD; Zhang et al. 2017) is a dataset consisting of multi-year recordings of weather and air quality data across different locations in Beijing. The variables in consideration are temperature, pressure, and wind speed, and the values are recorded once per hour. We segment the data into sequences, each covering the recordings of a whole week. Please refer to the supplementary materials for additional details about data preprocessing.

Similar to our synthetic data experiment settings, we compare the CTFP and latent CTFP models against latent ODE and VRNN. The ODE-RNN is used as the recognition network for both latent ODE and latent CTFP, and GRU is used as the RNN unit in both ODE-RNN and VRNN. Details about the model architecture can be found in the supplementary materials.

The results are shown in Table 2. We report the exact negative log-likelihood (NLL) per observation for CTFP, and the (upper bound of) NLL estimated by the IWAE bound, using $K = 125$ samples of latent variables, for latent ODE, latent

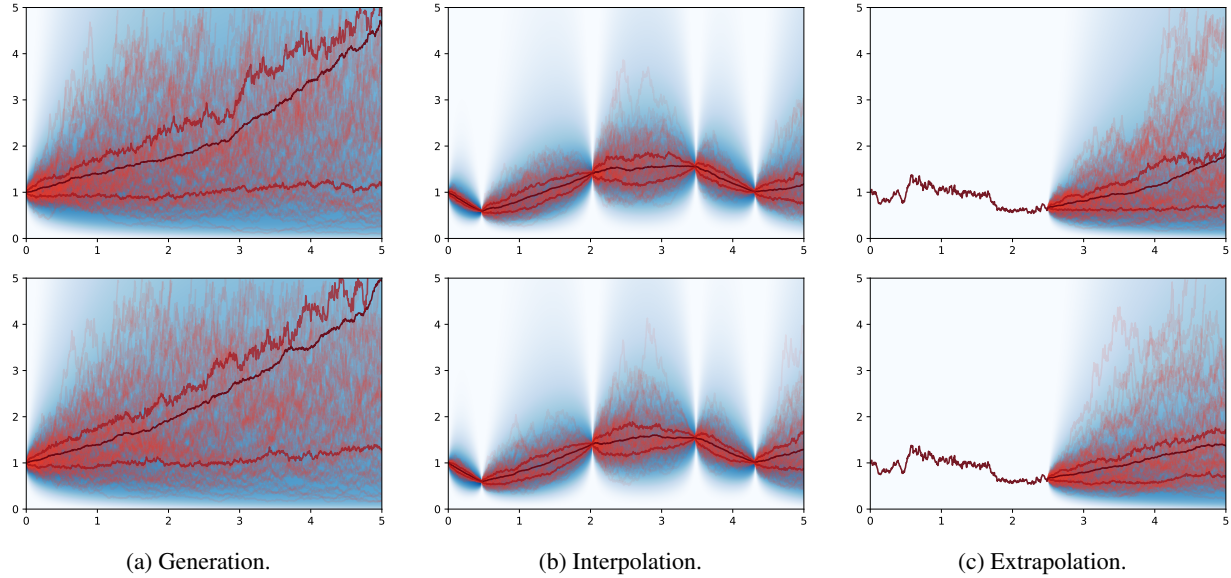


Figure 3. Comparison of CTFP to Geometric Brownian Motion. We compare (a) generation, (b) interpolation, and (c) extrapolation for CTFP (top row) and the geometric Brownian motion on which our model is trained (bottom row). Note our model’s ability to capture the skewed and non-Gaussian marginals of the underlying process. In addition to the sample trajectories (red) and the marginal density (blue), we also show the sample-based estimates of the inter-quartile range (dark red) and mean (brown) of the marginal density.

Model	Mujoco-Hopper (Rubanova et al., 2019)	BAQD (Bousseljot et al., 1995)	PTBDB (Zhang et al., 2017)
Latent ODE (Rubanova et al., 2019)	24.775 ± 0.010	2.789 ± 0.011	-0.818 ± 0.009
VRNN (Chung et al., 2015)	9.113 ± 0.018	0.604 ± 0.007	-1.999 ± 0.008
CTFP (ours)	-16.126 ± 0.166	-2.336 ± 0.035	-1.330 ± 0.028
Latent CTFP (ours)	-31.417 ± 0.059	-6.901 ± 0.026	-1.872 ± 0.006

Table 2. Quantitative Evaluation (Real-World Data). We show test negative log-likelihood on Mujoco-Hopper, Beijing Air-Quality Dataset (BAQD) and PTB Diagnostic Database (PTBDB) across different models. For CTFP, the reported values are exact; for the other three models, we report IWAE bounds using $K = 125$ samples. Lower values correspond to better performance. Standard deviations are based on 5 independent runs.

CTFP, and VRNN. For each setting, the mean and standard deviation of five evaluation runs are reported.

The evaluation results show that CTFP models outperform VRNN and latent ODE models on Mujoco-Hopper and BADQ datasets. On PTBDB, the performance of CTFP models is slightly worse than VRNN but better than latent ODE. One potential explanation is that the lack of continuity for ECG data invalidates our model assumptions.

It is worth noting that the latent ODE model in its original work (Rubanova et al., 2019) uses a fixed output variance and is evaluated using the mean squared error (MSE). We adapt the model to our tasks with a predicted output variance. We refer the readers to the supplementary materials for more details on the latent ODE model experiments.

Finally, Table 2 also suggests that the latent CTFP model consistently outperforms the CTFP model. This can be

regarded as an ablation study; it indicates that with the latent variables, the latent CTFP model is more expressive and able to capture the data distribution better.

5. Conclusion

In summary, we propose the continuous-time flow process (CTFP), a reversible generative model for stochastic processes, and its latent variant. It maps a simple continuous-time stochastic process, i.e., the Wiener process, into a more complicated process in the observable space. As a result, many desirable mathematical properties of the Wiener process are retained, including the efficient sampling of continuous paths, likelihood evaluation on arbitrary timestamps, and inter/extrapolation given observed data. Our experimental results demonstrate the superior performance of the proposed models on various datasets.

References

- Barber, D. *Bayesian Reasoning and Machine Learning*. Cambridge University Press, 2012.
- Baum, L. and Petrie, T. Statistical inference for probabilistic functions of finite state markov chains. In *The Annals of Mathematical Statistics*, 1966.
- Behrmann, J., Grathwohl, W., Chen, R. T., Duvenaud, D., and Jacobsen, J.-H. Invertible residual networks. In *International Conference on Machine Learning*, pp. 573–582, 2019.
- Bousseljot, R., Kreiseler, D., and Schnabel, A. Nutzung der ekg-signaldatenbank cardiodat der ptb über das internet. *Biomedizinische Technik/Biomedical Engineering*, 40(s1): 317–318, 1995.
- Bowman, S. R., Vilnis, L., Vinyals, O., Dai, A. M., Jozefowicz, R., and Bengio, S. Generating sentences from a continuous space. *arXiv preprint arXiv:1511.06349*, 2015.
- Burda, Y., Grosse, R., and Salakhutdinov, R. Importance weighted autoencoders. In *International Conference on Learning Representations*, 2019.
- Capp, O., Moulines, E., and Ryden, T. *Hidden Markov Models and Dynamical Systems*. Springer, 2005.
- Capp, O., Godsill, S., and Moulines, E. An overview of existing methods and recent advances in sequential monte carlo. In *Proceedings of the IEEE*, 2007.
- Chen, T. Q., Rubanova, Y., Bettencourt, J., and Duvenaud, D. K. Neural ordinary differential equations. In *Advances in neural information processing systems*, pp. 6571–6583, 2018.
- Chen, T. Q., Behrmann, J., Duvenaud, D. K., and Jacobsen, J.-H. Residual flows for invertible generative modeling. In *Advances in Neural Information Processing Systems*, pp. 9913–9923, 2019.
- Cho, K., van Merriënboer, B., Gulcehre, C., Bahdanau, D., Bougares, F., Schwenk, H., and Bengio, Y. Learning phrase representations using rnn encoder–decoder for statistical machine translation. In *Proceedings of the 2014 Conference on Empirical Methods in Natural Language Processing (EMNLP)*, pp. 1724–1734, 2014.
- Chung, J., Kastner, K., Dinh, L., Goel, K., Courville, A. C., and Bengio, Y. A recurrent latent variable model for sequential data. In *Advances in neural information processing systems*, pp. 2980–2988, 2015.
- Dinh, L., Krueger, D., and Bengio, Y. NICE: Non-linear independent components estimation. *arXiv preprint arXiv:1410.8516*, 2014.
- Dinh, L., Sohl-Dickstein, J., and Bengio, S. Density estimation using Real NVP. In *International Conference on Learning Representations*, 2017.
- Duane, S., Kennedy, A., Pendleton, B., and Roweth, D. Hybrid monte carlo. In *Physics Letters*, 1987.
- Dupont, E., Doucet, A., and Teh, Y. W. Augmented neural ODEs. In *Advances in Neural Information Processing Systems*, pp. 3134–3144, 2019.
- Durbin, J. and Koopman, S. J. *Time Series Analysis by State Space Methods*. Oxford University Press, 2012.
- Fox, E., Sudderth, E., Jordan, M., and Willsky, A. Non-parametric bayesian learning of switching linear dynamical systems. In *NeurIPS*, 2008.
- Fraccaro, M., Sønderby, S. K., Paquet, U., and Winther, O. Sequential neural models with stochastic layers. In *Advances in neural information processing systems*, pp. 2199–2207, 2016.
- Garnelo, M., Rosenbaum, D., Maddison, C., Ramalho, T., Saxton, D., Shanahan, M., Teh, Y. W., Rezende, D., and Eslami, S. A. Conditional neural processes. In *International Conference on Machine Learning*, pp. 1704–1713, 2018a.
- Garnelo, M., Schwarz, J., Rosenbaum, D., Viola, F., Rezende, D. J., Eslami, S., and Teh, Y. W. Neural processes. *arXiv preprint arXiv:1807.01622*, 2018b.
- Grathwohl, W., Chen, R. T. Q., Bettencourt, J., and Duvenaud, D. Scalable reversible generative models with free-form continuous dynamics. In *International Conference on Learning Representations*, 2019.
- Grimmett, G., Grimmett, G. R., Stirzaker, D., et al. *Probability and random processes*. Oxford university press, 2001.
- He, J., Spokoyny, D., Neubig, G., and Berg-Kirkpatrick, T. Lagging inference networks and posterior collapse in variational autoencoders. *arXiv preprint arXiv:1901.05534*, 2019.
- Hutchinson, M. F. A stochastic estimator of the trace of the influence matrix for laplacian smoothing splines. *Communications in Statistics-Simulation and Computation*, 19(2):433–450, 1990.
- Ito, K. and Xiong, K. Gaussian filters for nonlinear filtering problems. In *IEEE Trans. on Automatic Control*, 2000.
- J.M.Wang, D.J.Fleet, and A.Hertzmann. Gaussian process dynamical models for human motion. In *PAMI*, 2008.

- Julier, S. and Uhlmann, J. A new extension of the kalman filter to nonlinear systems. In *Aerospace/Defense Sensing, Simulation and Controls*, 1997.
- Kalman, R. A new approach to linear filtering and prediction problems. In *Journal of Basic Engineering*, 1960.
- Kim, H., Mnih, A., Schwarz, J., Garnelo, M., Eslami, A., Rosenbaum, D., Vinyals, O., and Teh, Y. W. Attentive neural processes. In *International Conference on Learning Representations*, 2019.
- Kingma, D. P. and Dhariwal, P. Glow: Generative flow with invertible 1x1 convolutions. In *Advances in Neural Information Processing Systems*, pp. 10215–10224, 2018.
- Kingma, D. P. and Welling, M. Auto-encoding variational bayes. In *International Conference on Learning Representations*, 2014.
- Kingma, D. P., Salimans, T., Jozefowicz, R., Chen, X., Sutskever, I., and Welling, M. Improved variational inference with inverse autoregressive flow. In *Advances in neural information processing systems*, pp. 4743–4751, 2016.
- Kobyzev, I., Prince, S., and Brubaker, M. A. Normalizing flows: Introduction and ideas. *arXiv preprint arXiv:1908.09257*, 2019.
- Lehrmann, A., Gehler, P., and Nowozin, S. Efficient nonlinear markov models for human motion. In *CVPR*, 2014.
- Li, X., Wong, T.-K. L., Chen, R. T., and Duvenaud, D. Scalable gradients for stochastic differential equations. *arXiv preprint arXiv:2001.01328*, 2020.
- Luo, R., Zhang, W., Xu, X., and Wang, J. A neural stochastic volatility model. In *Thirty-Second AAAI Conference on Artificial Intelligence*, 2018.
- Øksendal, B. Stochastic differential equations. In *Stochastic differential equations*, pp. 65–84. Springer, 2003.
- Papamakarios, G., Pavlakou, T., and Murray, I. Masked autoregressive flow for density estimation. In *Advances in Neural Information Processing Systems*, pp. 2338–2347, 2017.
- Papamakarios, G., Nalisnick, E., Rezende, D. J., Mohamed, S., and Lakshminarayanan, B. Normalizing flows for probabilistic modeling and inference. *arXiv preprint arXiv:1912.02762*, 2019.
- Pavlovic, V., Rehg, J., and MacCormick, J. Learning switching linear models of human motion. In *NeurIPS*, 2000.
- Rasmussen, C. *Gaussian Processes for Machine Learning*. MIT Press, 2006.
- Rezende, D. and Mohamed, S. Variational inference with normalizing flows. In *International Conference on Machine Learning*, pp. 1530–1538, 2015.
- Rubanova, Y., Chen, T. Q., and Duvenaud, D. K. Latent ordinary differential equations for irregularly-sampled time series. In *Advances in Neural Information Processing Systems*, pp. 5321–5331, 2019.
- Singh, G., Yoon, J., Son, Y., and Ahn, S. Sequential neural processes. In *Advances in Neural Information Processing Systems*, pp. 10254–10264, 2019.
- Srkk, S. On unscented kalman filtering for state estimation of continuous-time nonlinear systems. In *IEEE Trans. on Automatic Control*, 2007.
- Tassa, Y., Doron, Y., Muldal, A., Erez, T., Li, Y., de Las Casas, D., Budden, D., Abdolmaleki, A., Merel, J., Lefrancq, A., Lillicrap, T., and Riedmiller, M. DeepMind control suite. Technical report, DeepMind, January 2018. URL <https://arxiv.org/abs/1801.00690>.
- Zhang, S., Guo, B., Dong, A., He, J., Xu, Z., and Chen, S. X. Cautionary tales on air-quality improvement in beijing. *Proceedings of the Royal Society A: Mathematical, Physical and Engineering Sciences*, 473(2205):20170457, 2017.

A. Kolmogorov Extension Theorem

Let $(\Omega, \mathcal{F}, \mathbb{P})$ be a probability space. A continuous-time stochastic process is a measurable mapping $X : [0, \infty) \times \Omega \rightarrow \mathbb{R}^d$. A trajectory sampled from the process is a realization of this process. Continuous-time stochastic processes can also be viewed as infinite-dimensional random variables and are often characterized by finite-dimensional marginal distributions. For a collection of finite-dimensional distributions to consistently characterize a continuous-time stochastic process, the Kolmogorov extension theorem (Øksendal, 2003) states two sufficient conditions:

Exchangeability. Any finite-dimensional distribution should be consistent under permutations. More specifically, for any finite-dimensional distribution of $\{X_{\tau_1}, \dots, X_{\tau_n}\}$ and a permutation π of $\{1, \dots, n\}$, we have

$$p_{X_{\tau_1}, \dots, X_{\tau_n}}(x_{\tau_1}, \dots, x_{\tau_n}) \\ = p_{X_{\tau_{\pi(1)}}, \dots, X_{\tau_{\pi(n)}}}(x_{\tau_{\pi(1)}}, \dots, x_{\tau_{\pi(n)}}).$$

Marginalization Consistency. Marginalizing a subset of the dimensions results in a distribution that is consistent with the original one. For any $\{X_{\tau_1}, \dots, X_{\tau_n}\}$ and $1 \leq m \leq n$ we have,

$$p_{X_{\tau_1}, \dots, X_{\tau_m}}(x_{\tau_1}, \dots, x_{\tau_m}) \\ = \int \dots \int p_{X_{\tau_1}, \dots, X_{\tau_n}}(x_{\tau_1}, \dots, x_{\tau_n}) \, dx_{\tau_{m+1}} \dots dx_{\tau_n}.$$

B. Experimental Details for Latent ODE Models on Mujoco-Hopper Data

The original latent ODE paper focuses on point estimation and uses the mean squared error as the performance metric (Rubanova et al., 2019). When applied to our problem setting and evaluated using the log-likelihood, the model performs unsatisfactorily. In Table 3, the first row shows the negative log-likelihood on Mujoco-Hopper dataset. This is likely because the original latent ODE model uses a fixed output variance of 10^{-6} , which magnifies even a small reconstruction error.

To mitigate this issue, we propose two modified version of the latent ODE model. For the first version (V1), given a pretrained (original) latent ODE model, we do a logarithmic scale search for the output variance and find the value that gives the best performance on the validation set. The second version (V2) uses an MLP to predict the output mean and variance. Both modified versions have much better performance than the original model, as shown in Table 3, rows 2–3. It also shows that the second version of the latent ODE model (V2) outperforms the first one (V1) on the Mujoco-Hopper dataset. Therefore, we use the second version (V2) for all the experiments in the main text.

Model	NLL
Latent ODE (original)	$4 \times 10^7 \pm 9 \times 10^5$
Latent ODE (V1)	45.874 ± 0.001
Latent ODE (V2)	24.775 ± 0.010
VRNN	9.113 ± 0.018
CTFP	-16.126 ± 0.166
Latent CTFP	-31.417 ± 0.059

Table 3. Comparison of different version of latent ODE models on Mujoco-Hopper Datasets.

C. Model Architecture and Experimental Protocol

To ensure a fair comparison, we use the same values for important hyper-parameters like the latent variable and hidden state dimensions across all models. Likewise, we keep the underlying architectures as similar as possible and use the same experimental protocol across all models.

C.1. Model Architecture

For CTFP and Latent CTFP, we use a one-block augmented neural ODE module that maps the base process to the observation space. In the augmented neural ODE model, we use an MLP model consisting of 4 hidden layers of size 32–64–64–32 for both f and g in Equation 5. The same model architecture is used for both synthetic and real-world datasets. For latent CTFP and our modified latent ODE (V2) model, we use the same ODE-RNN model as the recognition network. For synthetic datasets, the ODE-RNN model consists of a one-layer GRU cell with a hidden dimension of 20 (the rec-dims parameter in its original implementation) and a one-block neural ODE module that has a single hidden layer of size 100, and it outputs a 10-dimensional latent variable. The same architecture is used by both latent ODE and latent CTFP models. For real-world datasets, the ODE-RNN architecture uses a hidden state of dimension 20 in the GRU cell and an MLP with a 128-dimensional hidden layer in the neural ODE module. The ODE-RNN model produces a 64-dimensional latent variable. For the generation network of the latent ODE (V2) model, we use an ODE function with one hidden layer of size 100 for synthetic datasets and 128 for real-world datasets. The decoder network has 4 hidden layers of size 32–64–64–32; it maps a latent trajectory to outputs of Gaussian distributions at different time steps.

The VRNN model is implemented using a GRU network. The hidden state of the VRNN models is 20-dimensional for synthetic and real-world datasets. The dimension of the latent variable is 64 for real-world datasets and 10 for synthetic datasets. We use an MLP of 4 hidden layers of size 32–64–64–32 for the decoder network, an MLP with one

hidden layer that has the same dimension as the hidden state for the prior proposal network and an MLP with two hidden layers for the posterior proposal network. For synthetic data sampled from Geometric Brownian Motion, we apply an exponential activation function to the output of all models.

C.2. Real-World Data Preprocessing Details and Downloadable Links

As mentioned in Section 4.2 of the paper, we pad all sequences into the same length and sample observation time-steps from a homogeneous Poisson process that is independent of the data. The sequence length of the Mujoco-Hopper dataset is 200 and the sequence length of Beijing Air-Quality dataset is 168. The maximum sequence length in the PTBDB dataset is 650. The observation scales are sampled from a homogeneous Poisson process with an intensity of 0.5. The Mujoco-Hopper, PTB Diagnostic Database and Beijing Air Quality datasets can be downloaded using the following links:

- <http://www.cs.toronto.edu/~rtqichen/datasets/HopperPhysics/training.pt>
- <https://www.kaggle.com/shayanfazeli/heartbeat/download>
- <https://archive.ics.uci.edu/ml/datasets/Beijing+Multi-Site+Air-Quality+Data>

C.3. Training Settings

For synthetic data, we train all models using the IWAE bound with 5 samples and a flat learning rate of 5×10^{-4} for all models. We also consider models trained with or without the aggressive training scheme proposed by He et al. (2019) for latent ODE and latent CTFP. We choose the best-performing model among the ones trained with or without the aggressive scheme based IWAE bound, estimated with 25 samples on the validation set for evaluation. The batch size is 100 for CTFP models and 25 for all the other models. For experiments on real-world datasets, we did a hyper-parameter search on learning rates over values of 5×10^{-4} and 10^{-4} , and whether using the aggressive training schemes for latent CTFP and latent ODE models. We report evaluation results of the best-performing model based on IWAE bound estimated with 25 samples.